Title

Self-assembled Camptothecin derivatives – Curcuminoids conjugate for combinatorial chemo-photodynamic therapy to enhance anti-tumor efficacy

Permalink

https://escholarship.org/uc/item/1835f9x9

Authors

Guo, Yiping
Liu, Hongmei
Xiao, Haijun
et al.

Publication Date

2021-02-01

DOI

10.1016/j.jphotobiol.2021.112124

Peer reviewed

Self-assembled Camptothecin Derivatives– Curcuminoids Conjugate for Combinatorial Chemo-Photodynamic Therapy to Enhance Anti-Tumor Efficacy

Yiping Guo [a, 1], Hongmei Liu [b, 1], Haijun Xiao [c,1], Minghao Yuan [b], Yushi Liu [b], Vladimír Sedlařík [c], Wei-Chun Chin [a, d], Juanru Liu [b], Li Guo [b, e*], Changqing Li [a, d*]

[a] *Quantitative and Systems Biology program, University of California, Merced, Merced, CA USA 95343*

[b] *School of Pharmacy, Chengdu University of Traditional Chinese Medicine, Chengdu, China 611137*

[c] *Centre of Polymer Systems, Tomas Bata University in Zlin, Zlin, Czech Republic 76001*

[d] *Department of Bioengineering, University of California, Merced, CA USA 95343*

[e] *State Key Laboratory of Characteristic Chinese Medicine Resources in Southwest China, Chengdu University of Traditional Chinese Medicine, Chengdu China, 611137*

[1] *Both authors contributed equally to this project.*

*Corresponding authors:

Prof. Changqing Li, Ph.D. (Email: cli32@ucmerced.edu)

Prof. Li Guo, Ph.D. (Email: guoli@cdutcm.edu.cn)

Abstract

Camptothecin (CPT), an alkaloid, was first discovered from plants and has potent anti-tumor activity. Since then, CPT analogs (namely Irinotecan and Topotecan) have been approved by the FDA for cancer treatments. Curcumin, on the other hand, is a widely used photosensitizer in photodynamic therapy (PDT) treatment. In our previous work, we have reported a straightforward strategy to construct a drug self-delivery system in which two-molecular species Irinotecan and Curcumin can self-assembly into a complex of ion pairs, namely ICN, through intermolecular non-covalent interactions. We found that ICN has slightly better chemotherapy efficacy than its individual components with much fewer side effects. In this paper, we aim to combine the chemotherapy and the PDT of ICN to further improve its anti-tumor performance. The efficient cellular uptake of ICNs was observed by confocal microscopy. Dichloro-dihydro-fluorescein diacetate (DCFH-DA) assay was used to detect the generation of singlet oxygen species. We found that the cell viability was 9% with both chemotherapy and PDT, and 31% with chemotherapy alone for the case with an ICN concentration of 10 μM, which demonstrated that the anti-tumor efficacy against the HT-29 cancer cell line was enhanced substantially with the combination therapy strategy. The study with an *in vivo* mouse model has further verified that the chemo-PDT dual therapy can inhibit tumor growth by 84% and 18.8% comparing with the control group and the chemotherapy group, respectively. Our results demonstrated that the new strategy using self-assembly and carrier-free nanoparticles with their chemo-PDT dual therapy may provide new opportunities to develop future combinatorial therapy methods in treating cancer.

Keywords: combination therapy, anti-tumor efficacy, photodynamic therapy, drug delivery system

Graphical abstract
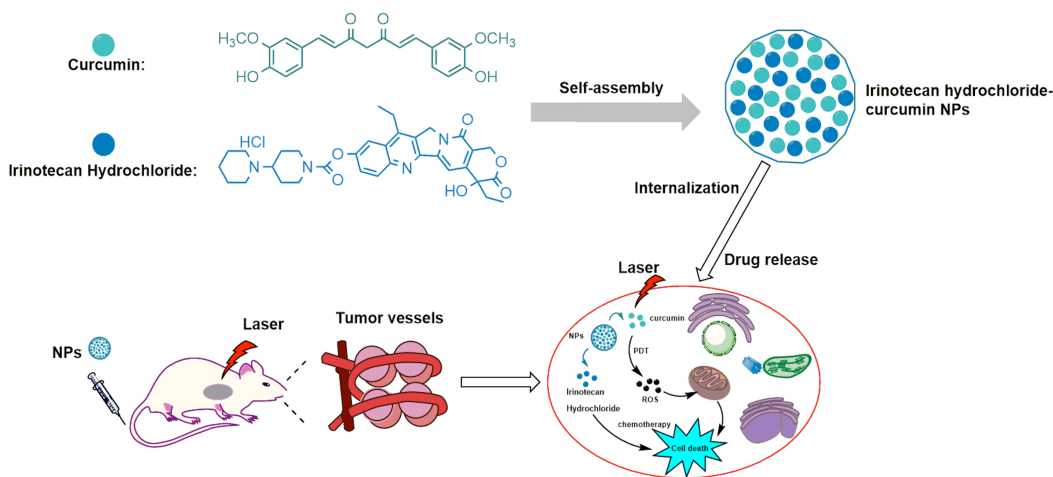
Introduction

Cancer is the second leading cause of death worldwide. As an extremely fatal disease, about 1 in every 6 deaths is due to cancer [1]. Surgery, chemotherapy, radiotherapy, and immunotherapy are the popular cancer treatments. However, multiple regulatory cell signaling pathways have been found defectively to compromise their treatment efficacy during the process of tumorigenesis including cell cycle arrest, apoptosis, or migration. Such cellular heterogeneity in cancer cells might cause limitations to combat this disease with mono-therapeutic approaches [2]. To address this issue, the combination therapy with the ability to suppress more than one pathway has reported improving the current treatments based on a synergistic therapeutic outcome [3,4,5,6]. The combination therapy strategy has already been utilized in the clinic, known as drug cocktail therapy. Studies have found that multi-pronged assault to tumors through administering a cocktail of different anti-cancer agents could achieve synergetic anti-tumor efficacy and minimize the severe side effects compared to the respective mono-therapeutic [7,8].

Recently, photodynamic therapy (PDT) is widely recognized as a promising alternative cancer treatment modality due to its painless and noninvasive administration process [9]. During the treatment, a photosensitizer is administered to patients and followed by the illumination with a light source at the tumor site. The light can activate the photosensitizer localized in the tumor site and then react with intracellular oxygen to form cytotoxic reactive oxygen species (ROS) [10]. Based on the PDT process, it can eradicate tumor tissue at low risk and in a controlled manner.

The side effect of PDT is relatively low because it is believed that the photosensitizer is not toxic until excited by the light. The major limitation is the challenges in delivering the light into deep tumors due to strong optical scattering and absorption. One strategy to overcome this limitation is to use high energy photons like x-rays to excite the photosensitizers [11]. Another method is to use a light guidance or catheter to deliver light into deep tissues directly [12]. Many other approaches have recently been introduced to overcome the drawbacks of PDT. [13,14,15]

Curcuminoids are bioactive compounds obtained from the plant *Curcuma longa*. One of its bioactive ingredient curcumin has been used as the photosensitizer of PDT [16,17]. Curcuminoids have many features, such as the blue region absorption, the long-wavelength cation photo-polymerization, and minimal cell cytotoxicity to normal cells, which make curcumin an ideal candidate as photosensitizers in PDT. Although curcumin has the potential to be a good photosensitizer candidate for efficient PDT, some limitations are preventing it from being widely utilized in the clinic. One drawback is its poor water solubility [18]. Another drawback is its instability under physiological conditions. In our previous study [19], we have reported a straightforward strategy to construct an easy manufactured drug self-delivery system in which two-molecular species Irinotecan and Curcumin can self-assemble into a complex of ion pairs, through intermolecular non-covalent interactions. The nano-self-assembly has been proven to be effective in delivering aqueous insoluble small molecules so that the water solubility of curcuminoids is improved substantially and the lactone hydrolysis of camptothecin derivatives remain activated in pharmacologically active forms [20].

Our previous work has proved that the nano-self-assembly has better chemotherapy efficacy with much fewer side effects compared with the individual components. However, its efficacy as a PDT photosensitizer has not been explored. In this paper, we report our studies on these two studies. Briefly, we would like to introduce ICN as an effective anti-tumor agent. The formulation of ICN is composed of a chemotherapy drug irinotecan and photosensitizer curcumin for combinatorial chemo-photodynamic therapy (Fig. 1). Because of the efficient cellular localization and abundant ROS generation, ICN has proved to be a good candidate as the multi-therapeutic agent. In this paper, we report the methods in section 2, the results in section 3, and conclude the paper in section 4 with some discussions.
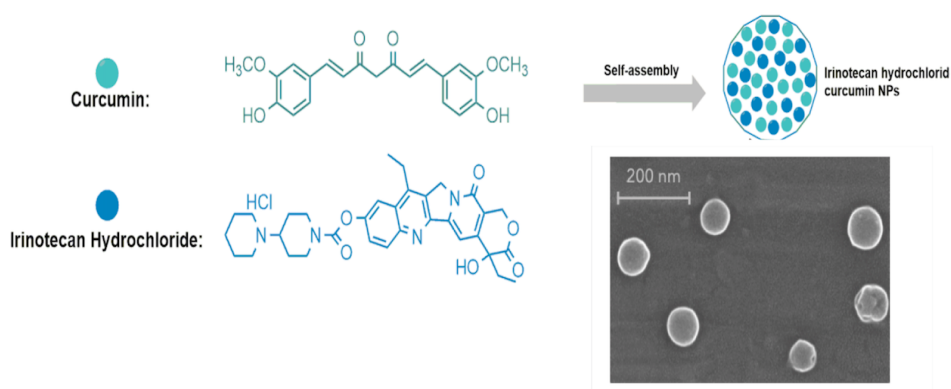
Figure 1. The formulation of self-assembled irinotecan hydrochloride-curcumin nanoparticles (ICN)

2. Methods

2.1 Materials

Irinotecan hydrochloride, curcumin, poloxamer 105, mannitol, dimethyl sulfoxide (DMSO), and DMEM Mixture F-12 Ham (DMEM/F12) were purchased from Sigma-Aldrich (St Louis, MO, USA) and used as received. Phosphate Buffered Saline (PBS, pH = 7.4) was prepared in the lab and ultrapure water was produced using a Milli-Q integral water system (Millipore, MA, USA). MitoTracker Red CMXRos was purchased from Beyotime Biotechnology Inc (P.R. China). Annexin V apoptosis detection kit FITC and ROS detection kit were purchased from KeyGEN Biotech (Nanjing, P.R. China). Penicillin–streptomycin, fetal bovine serum, and trypsin were purchased from Gibco (Grand Island, NY, USA)

2.2 Preparation of ICN

ICN was synthesized and purified as described in our paper [19]. Briefly, irinotecan hydrochloride and curcumin (ICN) were prepared based on an anti-solvent precipitation method. Typically, irinotecan hydrochloride (6.2 mg) and curcumin (3.7 mg) (Molar ratio I:C is about 1:1) were dissolved DMSO (300 μL) at room temperature, in which 1.5 mg of injectable non-ionic surfactant poloxamer 105 was added. The obtained organic solution was added into ultrapure water (30 mL) with magnetic stirring (500 RPM; 5 min) at room temperature.

2.3 Cytotoxicity assay

HT-29 cells were incubated in DMEM/F12 medium, where 10% FBS and 100 U (per mL) penicillin-S. were added. The cells were then seeded on 96-well plates with a density of 1×10^4 per well with DMEM/F12 medium and incubated in a humidified incubator containing 5% CO_2 at 37 °C for 24 h. After removal of the original medium, the cells were treated with various concentrations of Curcumin, Irinotecan hydrochloride, and ICNs for 4 h incubation. Then, the cells were washed with PBS and fresh medium twice and then exposed to 480 nm pigtailed laser diode (80 mW/ cm^2, 5 min). After incubation for 12 h, the cells were incubated with 20 μL MTT (5 mg/mL) for 4 h. Solutions were removed and followed by treatment with 150 μL DMSO to dissolve the formazan crystals. The absorbance was set at 490 nm using Elx800 Universal Microplate Reader (BioTek Instruments Inc., Winooski, VT, USA). The errors were calculated from two independent sets of experiments, in each of which six replicate wells were run for each concentration.

2.4 Detection of Intracellular ROS

HT-29 cells were plated in 12-well plates at the density of 1×10^5 cells per well for 24h at 37°C. After incubation with Curcumin and ICNs (5 μM of free Cur equivalent) for 4 h, the cells were washed twice with PBS buffer to remove excess. Each well was exposed to a 480-nm laser diode (power density 80 mW/cm^2) for 5 min at the same distance to deliver the same power. After incubation for 12 h, the cells were washed. Then 700 μL of 10 μM DCFH-DA was added to the cell suspension and incubated for 20 min at room temperature. The fluorescence signals were measured by flow cytometry and analyzed by Cell Quest software (Becton Dickinson FACSVerse).

2.5 Cellular localization of drugs

HT-29 cells were seeded on a glass-bottom petri dish at a concentration of 5×10^3 cells (per mL) for 12 h. After that, the cells were incubated with curcumin of 5 μM and ICN (equaling to Cur.) suspension for 4 h. After being washed two times with PBS, the cells were stained with Mitotracker Red (0.2 μM) reagent in live-cell imaging solution at room temperature for 30 min. The cells were then washed twice with PBS and placed under Leica SP8 X confocal microscope for imaging. Laser sources at 488 nm and 552 nm were used for the capture of curcumin, ICN, and MitoTracker, respectively.

2.6 Fluorescence-based Distribution and Uptake

HT-29 cells were seeded in confocal dishes and cultured in DMEM/F12 medium for 12 h. ICN suspension (equaling to 50 μM of Irinotecan hydrochloride) was then added into each dish and incubated in media with pH of 6.7 and 7.5 for 3 h before being measured by a Leica SP8 X confocal laser scanning microscope (excitation wavelength of 488 nm; Emission wavelength of 490-552 nm)

2.7 Apoptosis Analysis

Cell apoptosis was measured using Annexin V–FITC (fluorescein isothiocyanate)/PI (propidium iodide) Apoptosis Assay Kit. HT-29 cells were seeded in 12-well plates for 24 h at the density of 1×10^5 per well and incubated with 5 μM free Curcumin and ICN for 4 h. Then, each well was washed with PBS buffer twice and exposed to 480 nm laser diode for 5 min (power density 80 mW/cm^2). After incubation for 12 h, the cells were washed and fixed in 500 μL of Annexin V binding buffer containing 5 μL Annexin V-APC and 5 μL PI. After incubated at room temperature for 15 min in the dark, the cells were assessed for the status of apoptosis with FACS Calibur flow cytometer (Becton Dickinson, USA).

2.8 *In vivo* Therapeutic Efficacy

Male BALB/c nude mice, aged 5 weeks (20–25 g), were purchased from Dashuo experimental animals Co., Ltd. (Chengdu, China). All animal experiments were conducted under the guidelines approved by the Institutional Animal Care and Use Committee (IACUC) of Chengdu University of Traditional Chinese Medicine. The HT-29 tumor-bearing mice were randomly divided into three groups (Saline solution, Curcumin, and ICN) with equivalent tumor volume (around 100 mm^3), and were injected intravenously irinotecan hydrochloride (0.2μM kg per mouse) or ICN (equivalent irinotecan 0.2μM/kg per mouse) every three days for consecutive 21 days. All mice were fed in a dark room. For PDT experiments, the tumor site was illuminated by a 480-nm light source for 20 mins with a power density of 80 mW/cm^2. The PDT was implemented every three days and lasted for 15 days. Tumor volume was measured every third day and calculated as following: Tumor volume = length × width^2/2. Mice were sacrificed after 7 days of medication discontinuation. Tumors were excised, weighed and photographed.

2.9 Statistical Analysis

All quantitative data are shown as mean±SD, n≥3. Statistical analysis was conducted using GraphPad Prism t-test calculator and *p<0.05, **p<0.01, ***p<0.001.

3. Results

3.1 Formation Mechanism and Characterization of ICN

Curcumin and irinotecan hydrochloride self-assemble into complexes of ion pairs in polar organic solvents through intermolecular interactions. The chemical structures of environmental pH-dependent hydrolysis equilibria of irinotecan hydrochloride, and the chemical structures of curcuminoids in enol-keto tautomeric equilibria were shown in Fig. S2. The dissociation equilibria between curcuminoids and their anions were shown in Fig. S3. After the formation of ICN, we have observed the dispersion stability of ICN by changing their environmental pH values. The dispersion stability-time profiles have been provided in Fig. S1, from which we see that ICN nanoparticles under PBS (acidic), PBS (neutral) and DMSO conditions have no changes, demonstrating their good stability. The change of color in PBS (alkaline) indicates the possible hydrogen bonding between these two molecular species. Finally, we measured and normalized the fluorescence spectra of ICN, curcumin and irinotecan hydrochloride as shown in Fig. S6.

3.2 *In Vitro* Cytotoxicity

We first assessed the cytotoxicity of the Irinotecan and ICN induced anti-tumor efficacy in HT-29 cells (Fig. 2A). Cell viability studies under two different cancer treatments were performed to estimate cytotoxicity and anti-cancer efficacy on HT-29 cells. A significant decrease in HT-29 cell survival was observed at low concentrations (< 6.25 μM). However, the cytotoxicity can hit the therapeutic 'plateaus' while doubling the dosage of chemotherapy agents. The ICN group stalled out to 30% of cell viability even when the concentration of ICN increased to 8 times higher (50 μM). To overcome the anti-cancer drug resistance, we investigated the anti-cancer efficacy of Irinotecan and ICN in combination with photodynamic therapy. As shown in Figs. 2B and 2C, with or without laser irradiation, the curcumin group and Irinotecan group exhibited negligible differences in cell cytotoxicity to HT-29 cells in all concentrations. However, after having been exposed to laser, for the treatments with 2.5 μM and 5 μM of ICN, the viabilities of HT-29 cells

were 57% and 21%, respectively. When HT-29 cells were treated with 10 μM ICN in the combination of laser-induced PDT, the therapeutic 'plateau' was significantly brought down to 9%. ICN showed great cytotoxicity to HT-29 at low concentration but remained on 'the plateaus' of anti-cancer efficacy of around 33% at high concentration. With the combination of two treatments (ICN+PDT), a huge decrease of HT-29 cell viability was observed in Fig. 2C. This result verified that the combination treatments can achieve better anti-tumor efficacy than an individual treatment alone.
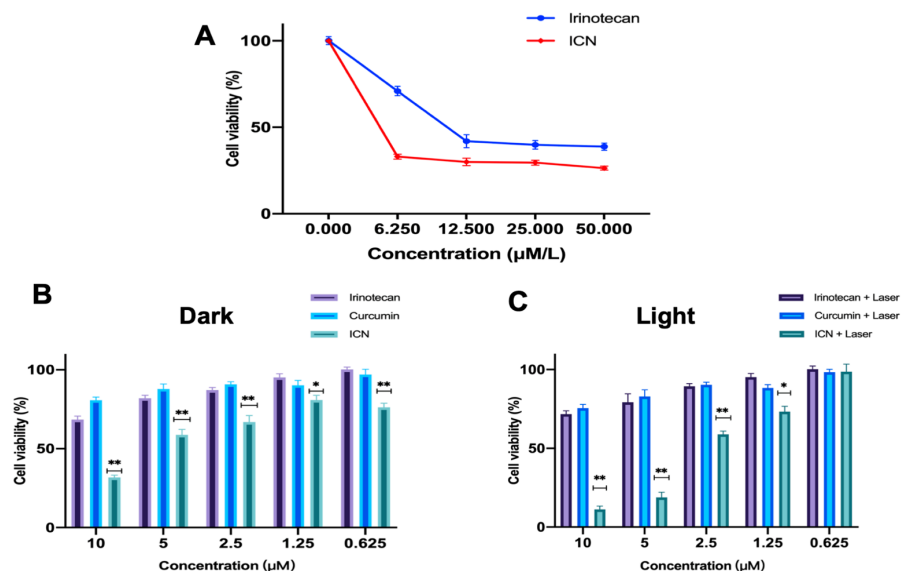
Figure 2. (A) *In vitro* cytotoxicity of Irinotecan and ICN in HT-29 cells. Cell viabilities of the HT-29 cells treated with Irinotecan, Curcumin, and ICN in the dark (B), and with laser exposure (C).

The *in vitro* cytotoxicity of ICN under various pH values were investigated on HT-29 cells (Fig. S5). Compared to free irinotecan hydrochloride, the *in vitro* cytotoxicity of ICN is largely improved as forming nanoparticles as demonstrated in Fig. S5. Furthermore, we also see that acidic environments result in better *in vitro* cytotoxicity of ICN on HT- 29 cells than alkaline condition.

3.3 ROS Generation

In PDT, the photosensitizers are transferred from the ground state into an excited state under a specific wavelength of the light source. The excited photosensitizers can react with molecular oxygen and generate cytotoxic ROS to induce oxidative damage or cell death [21]. We measured intracellular ROS generation by staining with DCFH-DA assay. As shown in Fig. 3, no obvious change can be found in ROS generation for the groups in the dark. When HT-29 cells were exposed to illumination (480 nm), there was a remarkable difference in ROS generation. ICN group could produce much more ROS (36.6%) than curcumin (3.39%). The quantification of intracellular ROS can be found in Fig. S7. This result indicated that increasing intracellular ROS was induced by the photochemistry activation between laser and ICN, resulting in better therapeutic efficacy in killing cancerous cells.
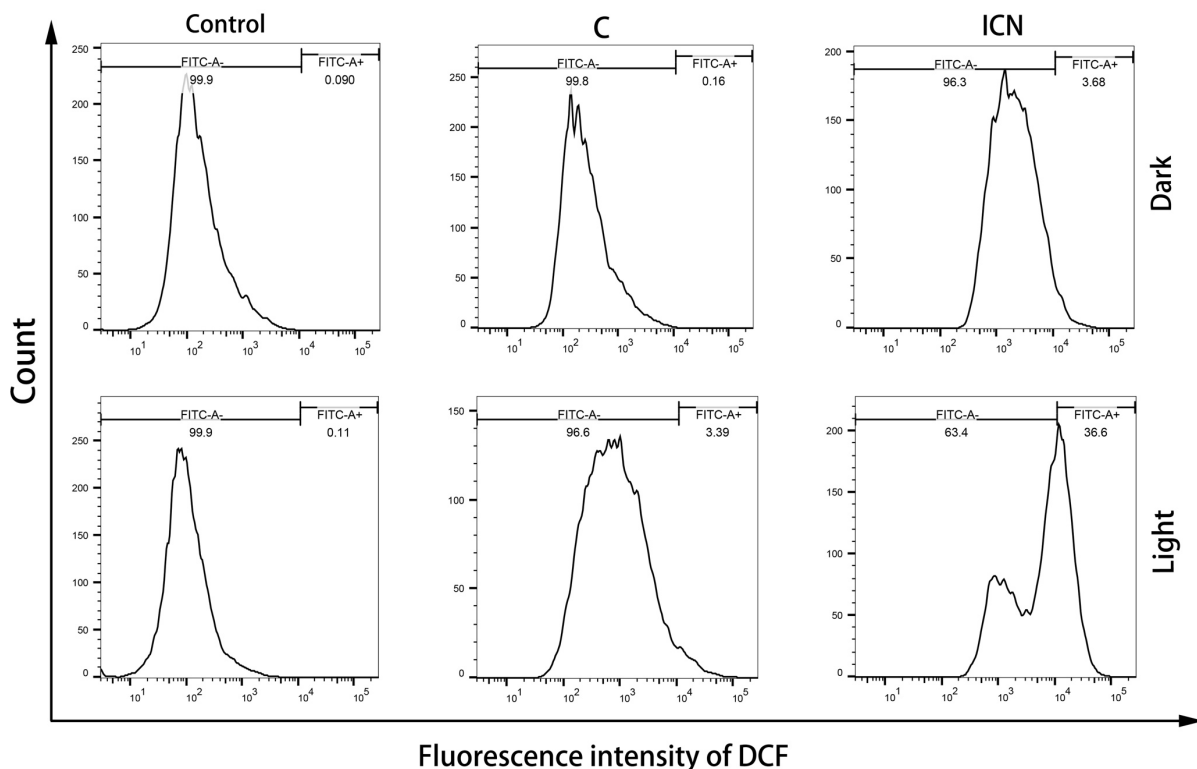

Figure 3. Effect of curcumin/ ICN-photodynamic treatments on intracellular ROS generation in HT-29 cells. The cells were stained with DCFH-DA before flow cytometric analysis.

3.4 Cellular Localization of Drugs

Among all cell organelles, mitochondria were frequently reported as the target site of singlet oxygen to improve the PDT efficacy [21]. The organelle mitochondria have been reported to be

the most effective subcellular targets in PDT because ROS-induced mitochondrial DNA damage results in cytotoxicity in the PDT treatment [22]. Therefore, the desirable photosensitizers or their delivery carriers are usually expected to be accumulated within or stay close to mitochondria [23]. To verify the mitochondria-targeting capabilities of ICN, we investigated it by incubating the curcumin-treated HT-29 cells and ICN treated HT-29 cells. As shown in Figure 4, cells treated with ICN show higher cellular uptake of ICN than curcumin in the mitochondria. The fluorescence-based distribution and quantified uptake efficiency of ICN and curcumin are shown in Fig. S8. This finding indicates that ICN is preferentially accumulated in mitochondria than curcumin, which demonstrates that ICN is a better photosensitizer than curcumin.
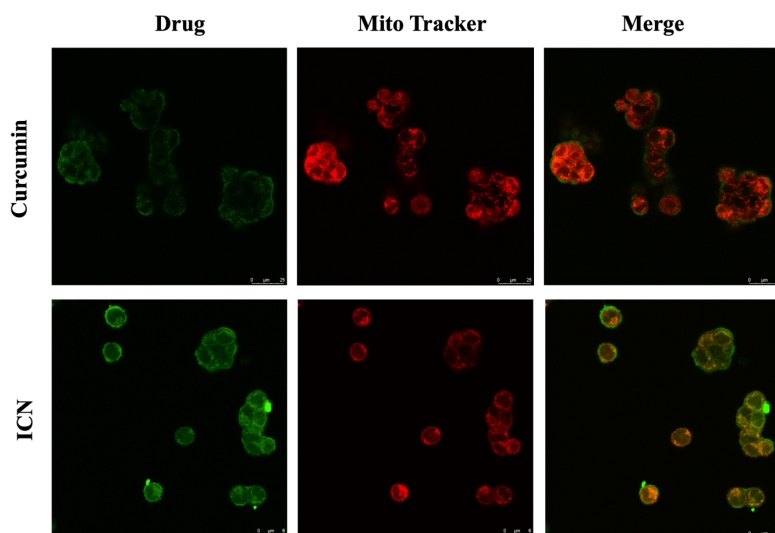

Figure 4. Confocal Laser scanning microscopy images of Cur and ICN (green), and Mitotracker Red (red) in HT-29 cell after incubation. Merged images of green and red channel refer to the co-localization levels of Cur and ICN with mitochondria. Scale bar is 25 μm.

3.5 Fluorescence-based Distribution under Different Environmental PHs

Fluorescence-based cellular uptake efficiency of ICN nanoparticles under environments with pH 6.7 and 7.5 was explored using HT-29 cells. As shown in Figure 5, the blank group where HT-29 cells alone under neutral conditions shows no fluorescence. For the ICN treated groups, cells under acidic environments (pH = 6.7) exhibit significantly stronger fluorescence than those in alkaline conditions (pH = 7.5), demonstrating a higher cellular uptake efficiency under acidic environments.

The tumor microenvironment is known to be acidic due to reasons of glycolytic cancer cell metabolism and cell hypoxia [24,25]. The preferential accumulation in acidic might explain why ICN can largely improve cellular toxicity in the tumoral microenvironment.
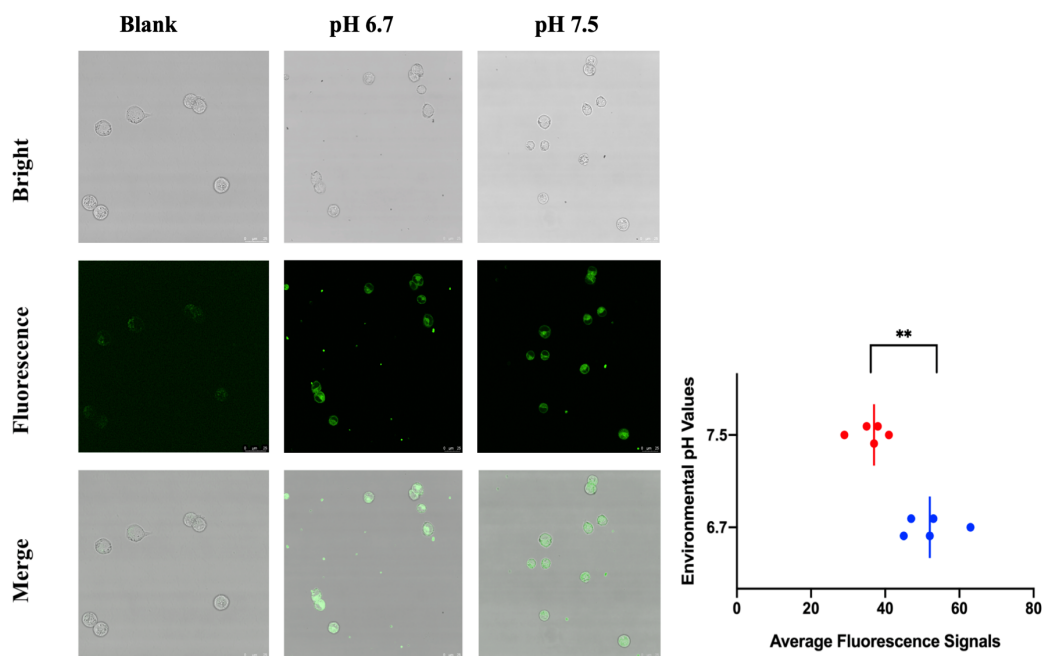

Figure 5. Fluorescence-based cellular uptake efficiency under different pH environments. For the group adding ICN, cells under acidic environment (pH = 6.7) show stronger fluorescence than those under alkaline environments (pH = 7.5). The significant difference is observed between groups with different environmental pH values. (**, $p < 0.01$)

3.6 Apoptosis Analysis by Annexin V-FITC/PI Staining

The percentage of apoptotic HT-29 cells was assessed by Annexin V-fluorescein isothiocyanate (FITC) and propidium iodide (PI) double staining for flow cytometry analysis. High Annexin V and low PI staining (Q3) indicated the early apoptosis of cells. On the other hand, strong staining signals of both Annexin V label and PI (Q2) showed the cells were in the stage of necrosis or late apoptosis [26]. As shown in Figure 6, 8.2% of illuminated HT-29 cells were found to be apoptotic (early apoptosis added late apoptosis) when incubated with curcumin. However, after treated with ICN, 41.16% (Q2 39.4% and Q3 1.76%) of the total cells were induced to apoptosis. This assay indicates that combined with PDT, ICN induced ROS mediated apoptosis in HT-29 cells.
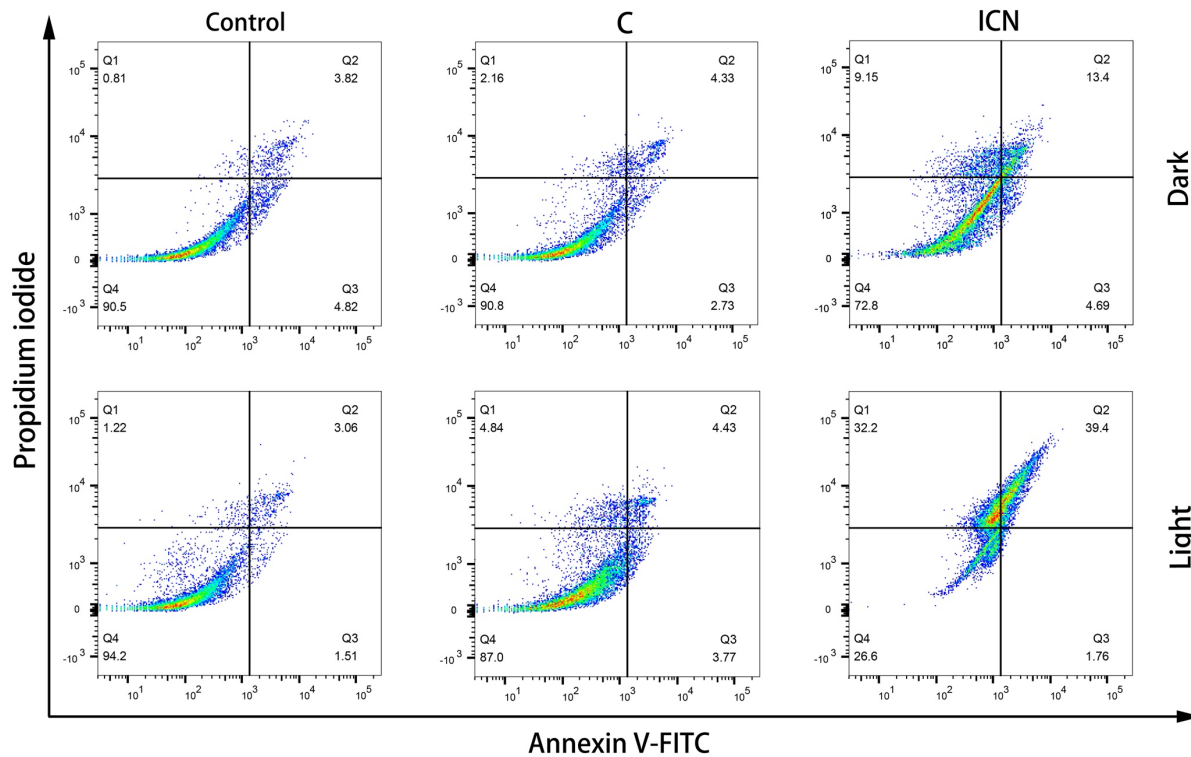
Figure 6. Fluorescence-activated cell sorter profiles of Annexin V-FITC/PI staining of HT-29 cells undergoing apoptosis induced by curcumin and ICN in the dark or with irradiation.

3.7 *In vivo* Therapeutic Efficacy

We evaluated the *in vivo* anti-tumor therapeutic efficacy with in vivo mice model. We randomly divided twelve tumor-bearing mice into three groups: PBS, ICN (without laser), and ICN (with laser). All mice were intravenously injected with either PSB or ICN with relatively equivalent tumor volume (~100 mm^3) and weight (20-25 g) at the dose of ICN 0.2μmol/kg to evaluate the anti-tumor efficacy. The medication was given every 3 days during a 15-day administration cycle. After the treatments, tumor volumes and body weights of each group were recorded, and the results are plotted in Fig. 7B for tumor volume and Fig. 7D for mice body weight. Mice were sacrificed 7 days after medication discontinuation. Tumors were excised out, photographed, and weighted as shown in Figs. 7A and 7 C. The tumor volume (V) was calculated as V = (the major widths of the tumor × the minor widths of the tumor^2)/2. The tumor volume of the PBS injection or the control group increased continuously to a volume of 1660 mm^3 on day 21. For the group with ICN injection without laser irradiation, due to chemotherapy alone, the tumor volume also slightly

shrank to 320 mm³ with a volume reduction of 80.7% compared with the control group. For the group with laser illumination and ICN drug injection, due to both chemotherapy and PDT, the tumor growth trend of the ICN- laser group declined significantly to 260 mm3 with a tumor volume reduction of 84.3% compared with the control group. We found that the tumor volume was further reduced by 18.8% due to PDT by comparing the ICN + Laser group with the INC group, which demonstrates that PDT was a significant complementary treatment along with chemotherapy. The results also verified the enhanced anti-tumor effect of ICN by applying both chemotherapy and PDT treatments. Furthermore, in this study, the body weights of mice in each group were recorded and showed no significant changes in all mice during the whole experimental period as shown in Fig. 7D, which indicates the risks associated with the Irinotecan (diarrhea and weight loss) are negligible. To understand further about the therapeutic effects, hematoxylin and eosin (H&E) staining images of tumors and major organs were obtained after various treatments (Fig. 8). There were no obvious cell morphology abnormality and cell damage found in the collected major organs. From H&E-stained sections of colon cancer from ICN treated groups, we observed the shrinkage of cells and the damage of cell nuclei (Fig. S4). These results demonstrate that ICN/laser combination therapy is safe for cancer treatment.
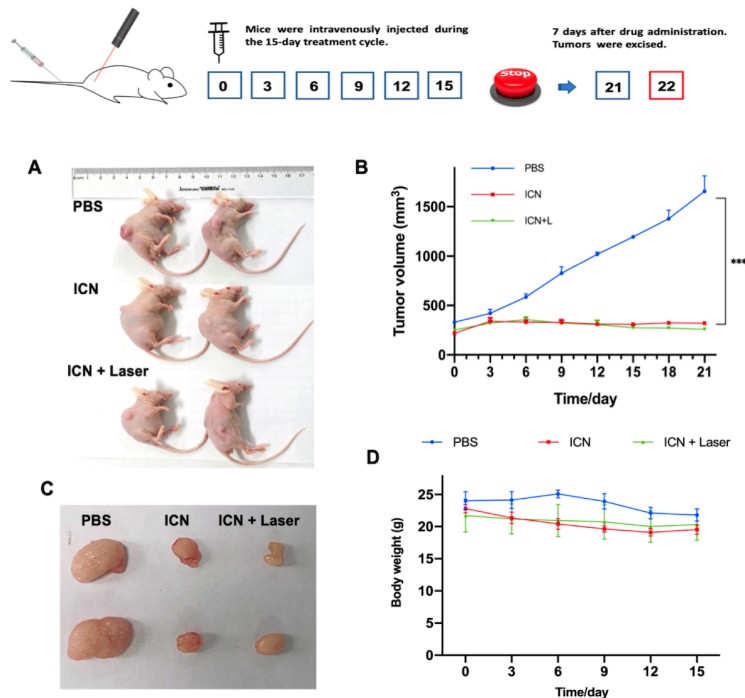
Figure 7. In vivo antitumor effect of HT-29 tumor-bearing mice were intravenously injected with ICN and PBS solution. Tumors were excised out, photographed, and weighted (A) and (C). ICN+L group were treated accompanying by illumination (80 mW /cm2). Compared with control, both ICN treated groups had antitumor effect and ICN + Laser group had the lowest tumor volume (B). Negligible changes of Body weight (D).
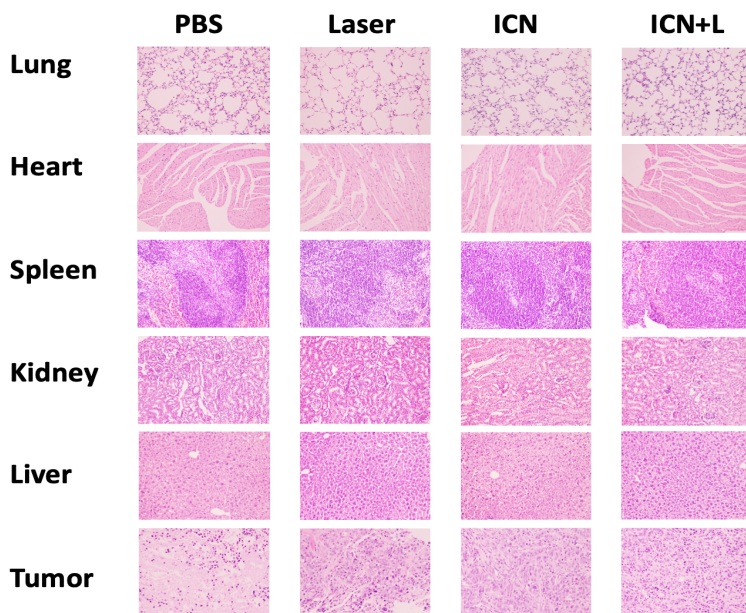

Figure 8. Hematoxylin and eosin (H&E) staining images of the main organs from different groups of mice after receiving with various treatments.

4. Conclusions

In summary, irinotecan hydrochloride and curcumin can form as a carrier-free nanoparticle (ICN) through a straightforward self-assembly approach. This unique nanoparticle not only overcame the hydrophobicity of curcumin but also enhanced the anti-tumor efficacy of irinotecan by integrating multiple treatment modalities. In this study, we found that ICN, as both the chemotherapy agent and the PDT photosensitizer, could enhance the cancer cell treatment efficiency when exposed to the light source. We found that this anti-tumor effect was caused by higher cellular uptake efficiency under acidic tumor microenvironments and subsequent intracellular ROS formation in the presence of diode laser irradiation. Altogether, our results indicate the potential of using ICN in the combination of chemotherapy and photodynamic therapy with synergistic anti-tumor efficacy.

Declaration

The authors state no conflict of interest.

Author contributions

Acknowledgments

References

[1] R.L. Siegel, K.D. Miller, A. Jemal, Cancer statistics, 2019. CA A Cancer J Clin, 69 (2019) 7-34. https://doi.org/10.3322/caac.21551

[2] M. O. Palumbo, P. Kavan, W. H. Miller, L. Jr. Panasci, S. Assouline, N. Johnson, V. Cohen, F. Patenaude, M. Pollak, R. T. Jagoe, G. Batist, Systemic cancer therapy: achievements and challenges that lie ahead, Front Pharmacol. 4 (2013) 57, https://doi.org/10.3389/fphar.2013.00057

[3] S. H. Chen, G. Lahav, Two is better than one; toward a rational design of combinatorial therapy. Curr. Opin. Struct. Bio. 41 (2016) 145–150. https://doi.org/10.1016/j.sbi.2016.07.020

[4] R. Bayat Mokhtari, T. S. Homayouni, N. Baluch, E. Morgatskaya, S. Kumar, B. Das, H. Yeger, Combination therapy in combating cancer. Oncotarget. 23 (2017) 38022–38043. https://doi.org/10.18632/oncotarget.16723

[5] Y. Wen, W. Zhang, N. Gong, Y. F. Wang, H. B. Guo, W. Guo, P. C. Wang, X. J. Liang, Carrier-free, self-assembled pure drug nanorods composed of 10-hydroxycamptothecin and chlorin e6 for combinatorial chemo-photodynamic antitumor therapy in vivo, Nanoscale 38 (2017) 14347–14356. https://doi.org/10.1039/c7nr03129g

[6] K. Zheng, H. Liu, X. Liu, Y. Wang, L. Li, S. Li, J. Xue, M. Huang, M, Tumor Targeting Chemo- and Photodynamic Therapy Packaged in Albumin for Enhanced Anti-Tumor Efficacy, Int. J. Nanomedicine. 15 (2020) 151–167. https://doi.org/10.2147/IJN.S227144

[7] B. Shrestha, L. Tang, G. Romero, Nanoparticles-Mediated Combination Therapies for Cancer Treatment. Adv. Therap., 2 (2019)1900076. doi:10.1002/adtp.201900076

[8] X. Li, J. Kim, J. Yoon, J. X. Chen, Cancer-Associated, Stimuli-Driven, Turn on Theranostics for Multimodality Imaging and Therapy. Adv. Mater. 29 (2017) 10.1002/adma.201606857. https://doi.org/10.1002/adma.201606857

[9] D. van Straten, V. Mashayekhi, H. S. de Bruijn, S. Oliveira, D. J. Robinson, Oncologic Photodynamic Therapy: Basic Principles, Current Clinical Status and Future Directions, Cancers, 2 (2017) 19. https://doi.org/10.3390/cancers9020019

[10] A. P. Castano, T. N. Demidova, M. R. Hamblin, Mechanisms in photodynamic therapy: part one-photosensitizers, photochemistry and cellular localization, Photodiagnosis Photodyn Ther. 4 (2004) 279–293. https://doi.org/10.1016/S1572-1000(05)00007-4

[11] Y. Guo, S. Sheng, M. C. Lun, S-M. Tsai, W-C. Chin, R. Hoglund, C. Li, Photodynamic therapy excited by Cerenkov Radiation from Cesium-137 irradiator*: in vitro* studies, Clin. Onco. Res., 3 (2020) 6. https://doi.org/10.31487/j.COR.2020.06.07

[12] M. H. Schmidt, D. M. Bajic, K. W. Reichert, T. S. Martin, G. A. Meyer, H. T. Whelan, Light-emitting Diodes as a Light Source for Intraoperative Photodynamic Therapy, Neurosurgery, 3 (1996) 552–557. https://doi.org/10.1097/00006123-199603000-00025

[13] X. Li, S. Yu, D. Lee, G. Kim, B. Lee, Y. Cho, B. Y. Zheng, M. R. Ke, J. D. Huang, K. T. Nam, X. Chen, J. Yoon, Facile Supramolecular Approach to Nucleic-Acid-Driven Activatable Nanotheranostics That Overcome Drawbacks of Photodynamic Therapy. ACS nano. 12 (2018) 681–688. https://doi.org/10.1021/acsnano.7b07809

[14] X. Li, S. Lee, J. Yoon, Supramolecular photosensitizers rejuvenate photodynamic therapy. Chem. Soc. Rev. 47(2018) 1174–1188. https://doi.org/10.1039/c7cs00594f

[15] X. Li, J. F. Lovell, J. Yoon, X. Chen, Clinical development and potential of photothermal and photodynamic therapies for cancer. Nat. Rev. Clin. Oncol. 17 (2020) 657–674. https://doi.org/10.138/s41571-020-0410-2

[16] A. Amalraj, A. Pius, S. Gopi, Biological activities of curcuminoids, other biomolecules from turmeric and their derivatives - A review. J Tradit Complement Med. 2 (2016) 205-233. https://doi.org/10.1016/j.jtcme.2016.05.005

[17] B. S. S. Vetha, E. Kim, P. Oh, S. Kim, S. Lim, M-H. Sojn, H-J. Jeong, Curcumin Encapsulated Micellar Nanoplatform for Blue Light Emitting Diode Induced Apoptosis as a New Class of Cancer Therapy, Macromol. Res. 27 (2019) 1179–1184 https://doi.org/10.1007/s13233-019-7168-3

[18] S. Jiang, R. Zhu, X. He, J. Wang, M. Wang, Y. Qian, S. Wang, Enhanced photocytotoxicity of curcumin delivered by solid lipid nanoparticles. Int. J Nanomedicine, 12 (2016) 167–178. https://doi.org/10.2147/IJN.S123107

[19] H. Xiao, Y. Guo, H. Liu, Y. Liu, Y. Wang, C. Li, J. Císař, D. Škoda, I. Kuřitka, L. Guo, V. Sedlařík, Structure-based design of charge-conversional drug self-delivery systems for better targeted cancer therapy, Biomaterials 232 (2020) 119701. https://doi.org/10.1016/j.biomaterials.2019.119701

[20] C. Ren, J. Zhang, M. Chen, Z. Yang, Self-assembling small molecules for the detection of important analytes, Chem. Soc. Rev. 43 (2014) 7257-7266

[21] A. P. Castano, T. N. Demidova, M. R. Hamblin, Mechanisms in photodynamic therapy: part two-cellular signaling, cell metabolism and modes of cell death. Photodiagnosis Photodyn Ther. 1 (2005) 1-23. https://doi.org/10.1016/S1572-1000(05)00030-X

[22] D. B. Zorov, M. Juhaszova, S. J. Sollott, Mitochondrial reactive oxygen species (ROS) and ROS-induced ROS release. Physiol Rev. 3 (2014) 909–950. https://doi.org/10.1152/physrev.00026.2013

[23] X. Gu, C. Shen, H. Li, E. M. Goldys, W. Deng, X-ray induced photodynamic therapy (PDT) with a mitochondria-targeted liposome delivery system, J. Nanobiotechnology, 1 (2020) 87. https://doi.org/10.1186/s12951-020-00644-z

[24] J. Chiche, M. C. Brahimi-Horn, J. Pouysségur, Tumour hypoxia induces a metabolic shift causing acidosis: a common feature in cancer, J. Cell. Mol. Med. 4 (2010) 771–794. https://doi.org/10.1111/j.1582-4934.2009.00994.x

[25] X. Lin, Y. Fang, Z. Tao, X. Gao, T. Wang, M. Zhao, S. Wang, Y. Liu, Tumor-Microenvironment-Induced All-in-One Nanoplatform for Multimodal Imaging-Guided Chemical and Photothermal Therapy of Cancer, ACS Appl. Mater. Interfaces, 28 (2019) 25043–25053. https://doi.org/10.1021/acsami.9b07643

[26] D. Wlodkowic, W. Telford, J. Skommer, Z. Darzynkiewicz, Apoptosis and beyond: cytometry in studies of programmed cell death, Methods Cell Biol. 103 (2011) 55–98. https://doi.org/10.1016/B978-0-12-385493-3.00004-8